Adaptive FEM-DEM simulation of a soft projectile impact on a reinforced concrete slab

Yury Novozhilov[1], Eric Piskula[2],

[1]CADFEM Germany GmbH
[2]Ansys Inc

1 Introduction

Modeling the behavior of reinforced concrete (RC) structures under the action of destructive loads, considering the non-linear material properties and the strain-rate effects is an indispensable part of calculations in the design of standard civil structures. The International Atomic Energy Agency (IAEA) prescribes these requirements for the design of buildings and structures of Nuclear Power Plants (NPP) [1].
A soft impact of a body imitating an aircraft engine projectile is considered according to experiments [2 – 7]. Such a study can determine the ability of RC structures to withstand the impact of an engine or other large aircraft fragment. The paper describes an approach to solving such a problem, especially for a large-thickness under-reinforced slab made of low-quality concrete. Such a combination of design parameters may prove challenging for FE modeling due to significant mesh distortions and the need to model material erosion.

2 Soft engine projectile

One of the distinctive features of the considered experiment series was the use of an abstract soft projectile and a real General Electric J79 jet engine (see Fig. 1) used on McDonnell Douglas F-4 Phantom II fighters. During their experimental work, the authors not only studied the impact of this engine on an RC slab but also created an equivalent simplified soft projectile (see Fig. 2), code-named LED (Large-Scale Equivalent Deformable).

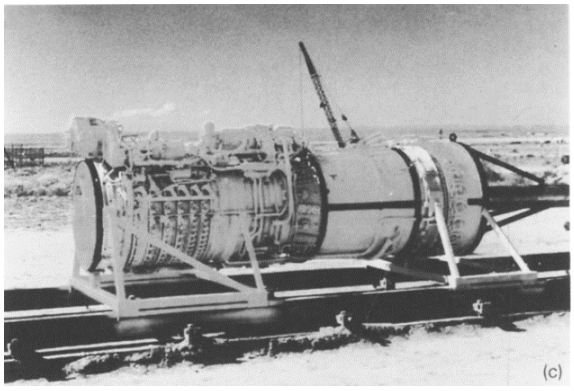

Fig.1: General Electric J79 engine

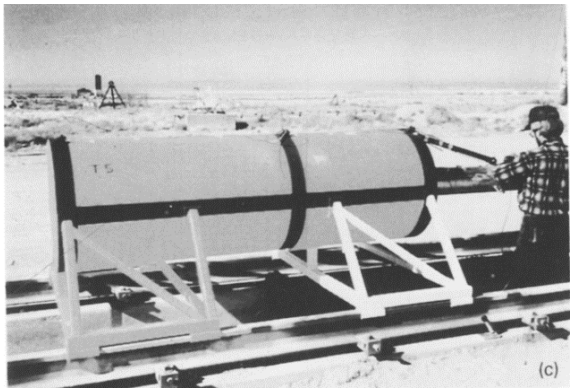

Fig.2: The LED soft projectile

The tests showed that the impact of the LED and the impact of the General Electric J79 jet engine are equivalent to the load transferred on a concrete slab. Thus, in the numerical modeling of this experiment, we do not need to create an accurate model of the General Electric J79. It is sufficient to develop and calibrate the FE model of the LED.
The LED consists of two connected pipes modeling the walls of the compressor and combustion chamber. These connected tubes have relatively thick disks at their ends: the compressor front frame, compressor rear frame, and turbine frame (see Fig. 3).

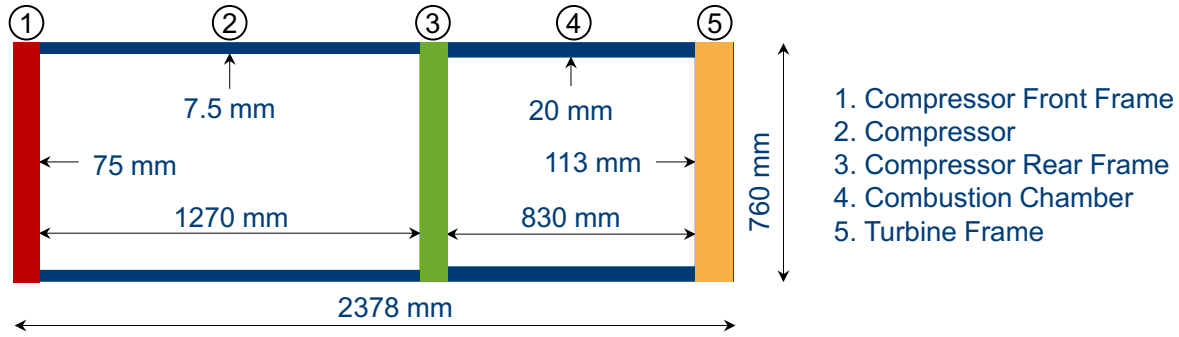

Fig.3: The LED dimensions and structure

The LED is made of steel with a known Yield Stress of 349.1 MPa and Ultimate Stress of 687.4 MPa. Assuming a failure strain of about 8%, we can reconstruct a smooth isotropic hardening curve for this material using Swift Law assumptions (see Fig. 4). This approach does not improve the accuracy of the calculations because we cannot obtain more data than we already have. However, using a smooth curve improves the overall material deformation stability. The total LED mass is 1420 kg. It is also mentioned that the model has an additional telemetry package with a 43 kg weight.

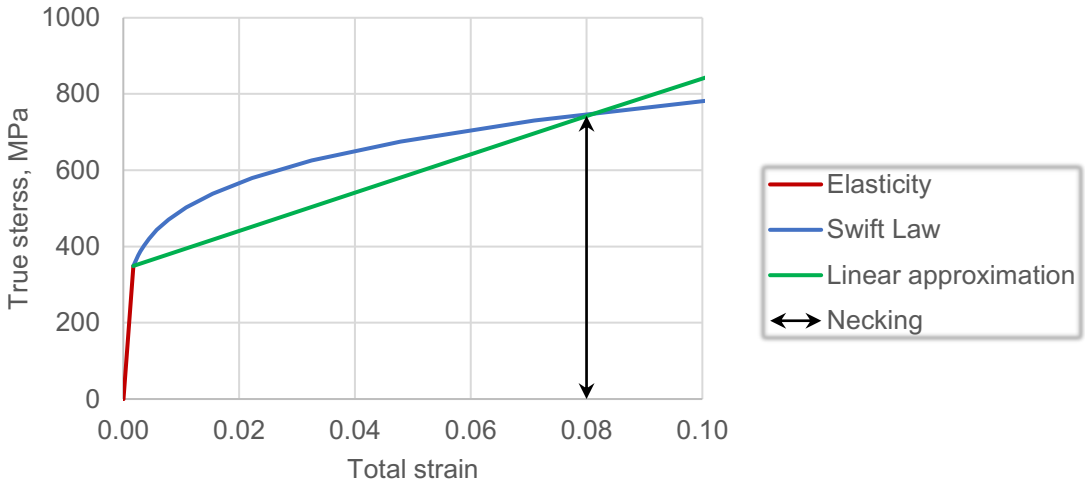

Fig.4: The LED material properties

The LED finite element (FE) model consists of two shell parts (Compressor and Combustion Chamber) and three solid parts (Compressor Front Frame, Compressor Rear Frame, and Turbine Frame) connected by **`*CONTACT_TIED_SHELL_EDGE_TO_SOLID`**. This contact allows solid parts with 3 DOF and shell parts with 6 DOF while maintaining moment balance.
Verification of the correctness of LED modeling is checked based on a comparison with the experiment's results on axial quasi-static compression of the model. Artificial defects have been introduced into the model (the shell radius has been increased by 1 mm in the illuminated region; see Fig. 5), ensuring stable buckling initiation under axial compression.

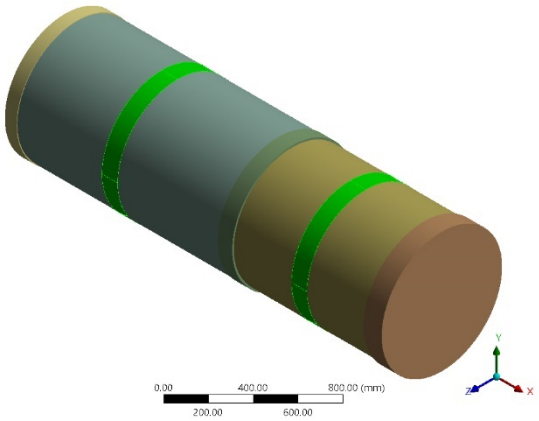

Fig.5: Artificial defect zones in the LED model (1 mm radios increment)

The deformation process and the resulting axial reactions are shown in Figures 6 and 7. The results were obtained for solid elements **`ELFORM = 1`** with a characteristic element size of 100 mm and shell elements **`ELFORM = 2`** with a characteristic element size of 50 mm and five integration points along the thickness. One second was simulated, and the deformation of the model was set to 1200 mm using **`*BOUNDARY_PRESCTIBE_MOTION_RIGID`** in combination with **`*DEFINE_CURVE_SMOOTH`**.

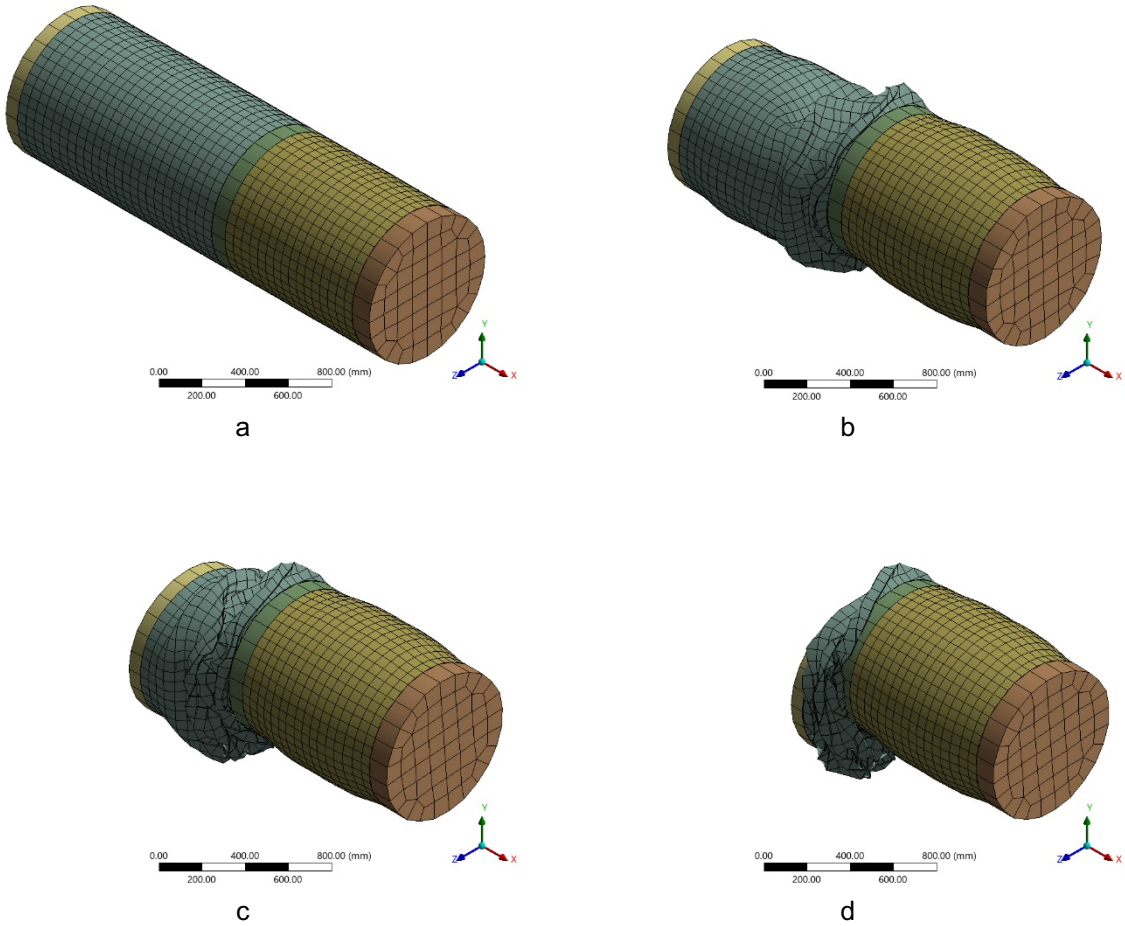

Fig.6: LED axial reformation process key frames: a – 0.00 s; b – 0.33 s; c – 0.66 s; d – 1.00 s

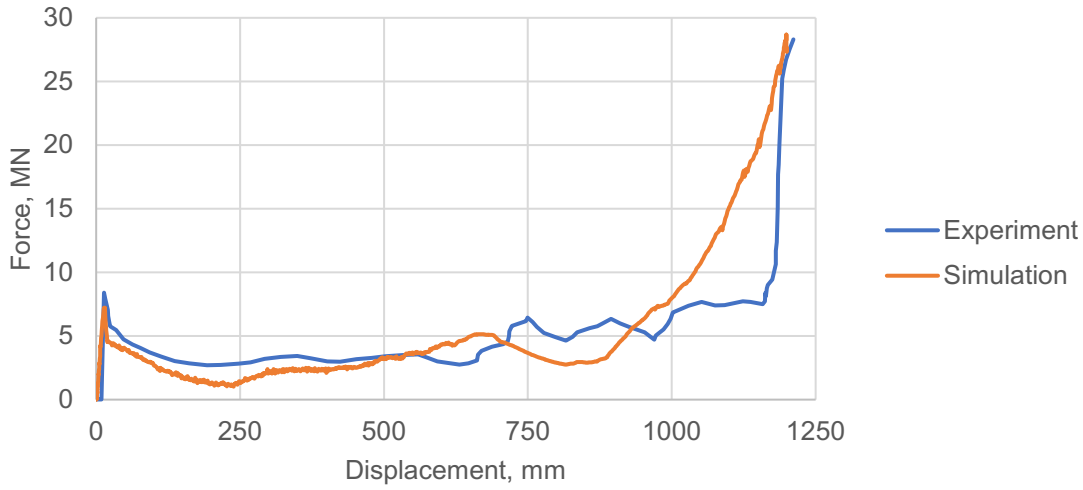

Fig.7: LED quasistatic compression test results

3 RC slab

3.1 Materials

Only one RC slab with a thickness of 1600 mm is tested for the LED impact. It is fixed vertically on the test bench with four anchors. The slab's characteristic dimensions are shown in figure 8. The concrete's uniaxial compressive strength is 23.5 MPa.

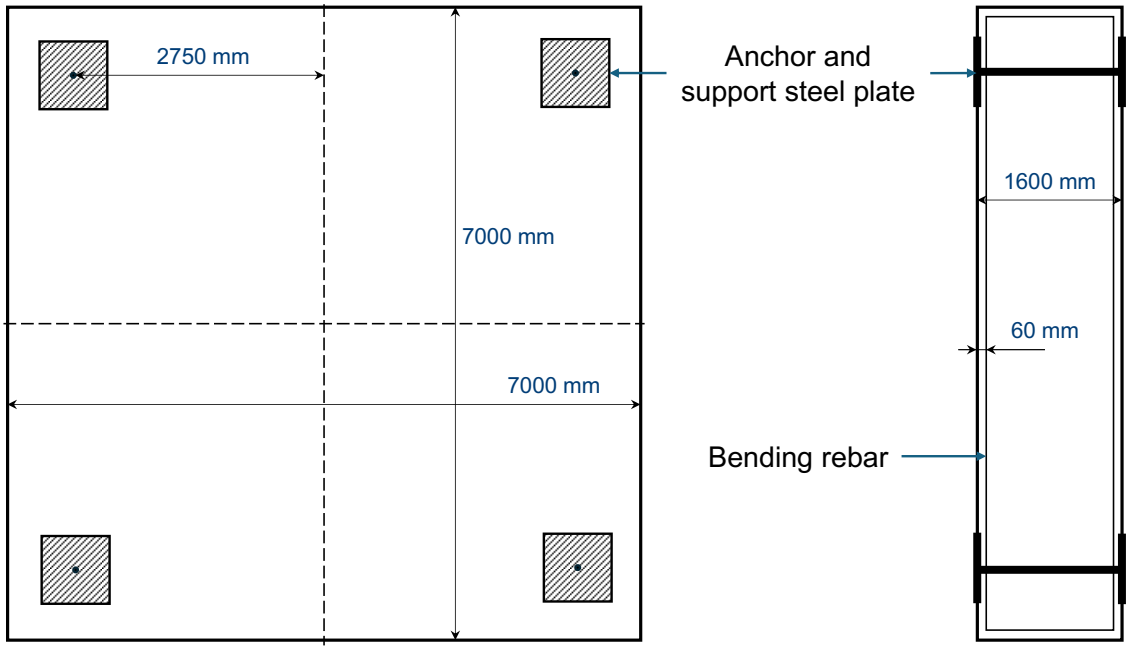

Fig.8: Test RC slab dimensions

The Continuous Surface Cap Model is a concrete material (see Table 1). This concrete model can be used for low-strength concrete using an updated high-precision parameter calibration procedure [8]. Standard easy input of ***MAT_CSCM_CONCRETE** is not designed for such a low concrete strength and will generate model with significant error in strength estimation. With the updated calibration procedure, all ***MAT_CSCM** model parameters (see Table 1) can be identified based on density, axial compressive strength, and fracture energy (which can be calculated based on the characteristic size of the aggregate). For this procedure's application, the aggregate's characteristic size is assumed to be 16 mm (the average value according to the CEB-FIP 1990 code).

Table 1: Continuous Surface Cap Model parameters for concrete material

```
*MAT_CSCM_TITLE
f_c = 23.5
$#     MID       RHO      NPLOT      INCRE      IRATE      ERODE      RECOV    ITRETRC
       159   2.4E-09          1          0          0       1.05         10          0
$#    PRED
         0
$#       G          K      ALPHA      THETA     LAMBDA       BETA         NH         CH
 1.313E+04  1.751E+04      5.773     0.3434      1.893    0.08061          0          0
$#  ALPHA1     THETA1    LAMBDA1      BETA1     ALPHA2     THETA2    LAMBDA2      BETA2
      0.82          0     0.2407    0.01427       0.76          0       0.26    0.01427
$#       R         X0          W         D1         D2
     2.533      61.55      0.065   0.000611 2.225E-06
$#       B        GFC          D        GFT        GFS       PWRC       PWRT       PMOD
       100      6.602        0.1    0.06602    0.06602          5          1          0
$# ETA_0_C        N_C    ETA_0_T        N_T      OVERC      OVERT     SRATE      REPOW
  0.000107       0.78 5.678E-05       0.48      19.45      19.45          1          1
```

The model's reinforcement step is 200 mm, with a concrete cover of 60 mm. Two parameter sets are given for the reinforcement material (see Table 2). By averaging these values and using Swift Law with the assumptions described above, we can reconstruct a smooth plastic hardening curve for the reinforcement material (see Fig. 9). The same material will be used for anchors and supporting steel plates.

Table 2: Rebar characteristics

Rebar diameter, mm	32.3	35.8
Yield Strength, MPa	488.7	466.5
Ultimate Strength, MPa	744.5	732.9

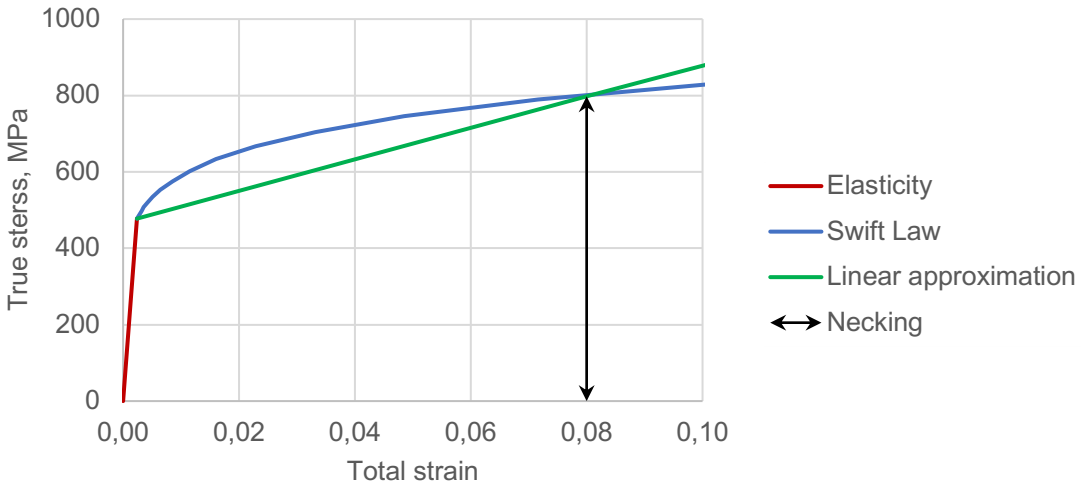

Fig.9: Rebar material properties

All steel elements of the slab are modeled with **`*MAT_PIECEWISE_LINEAR_PLASTICITY`**. According to IAEA recommendations, the strain-rate effects are accounted for using the Couper-Simonds model ($C = 40\ s^{-1}$, $p = 5$) in the case of experimental data absence [9].

3.2 FE mesh, loads, and boundary conditions

The model of an RC slab consists of a combination of different types of elements. The CSCM model is susceptible to the tuning of hourglass controls. Using **`IHQ = 6`** with QH coefficients larger than 0.03 can cause unphysical and asymmetric damage accumulation in the material. So, hexahedral solid elements **`ELFORM = 1`** with **`IHQ = 6`**, **`QH = 0.01`** are used to model concrete (see Fig. 10a). Hughes-Liu beams with cross-section integration model steel anchor rods and reinforcing bars (see Fig. 10b, 10c). Belytschko-Tsay shell elements with three integration points and **`IHQ = 4`**, **`QH = 0.1`** are used for steel supporting plates (see Fig. 10c).

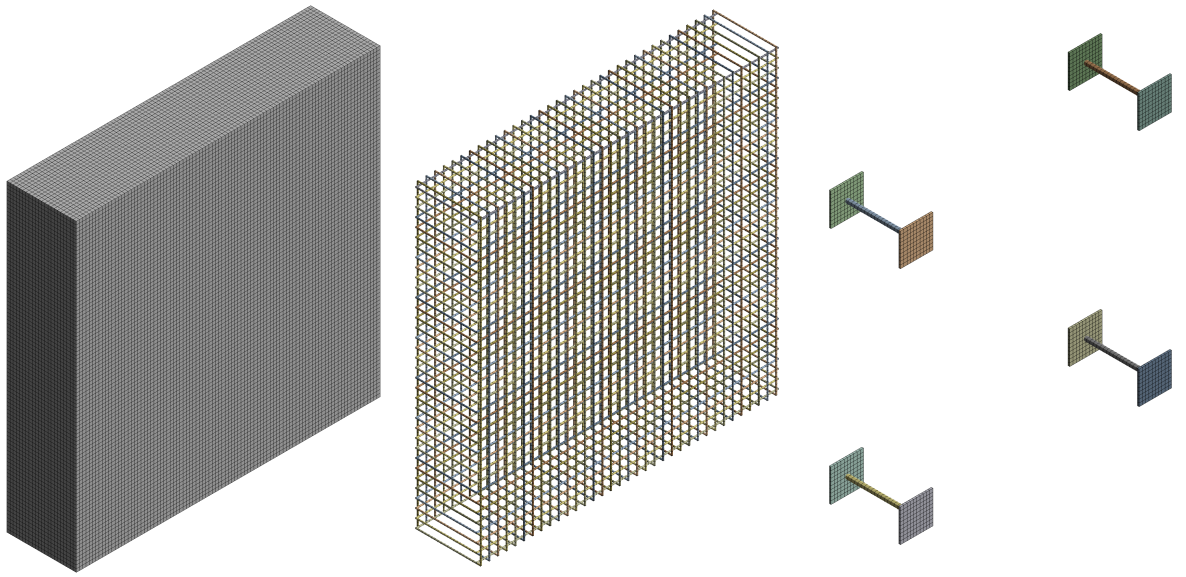

a b c

Fig.10: RC slab model parts: a – concrete; b – rebar; c – anchors with supporting steel plates

This paper investigates the effect of FE mesh size on the results. As shown in previous studies [10], when modeling RC under impact loads, the mesh size should not be larger than the reinforcement step (200 mm in this experiment). However, when using a mesh whose element size is smaller than the thickness of the protective layer (in this experiment, this value is 60 mm), a layer of solid concrete elements without reinforcement coupling is formed on the surface of the model, which significantly reduces the stability of the calculation and can lead to the collapse of the solution. Thus, we consider the results for models with characteristic element sizes of 200, 150, 100, 75, and 50 mm.
The simulation also studies the effect of concrete material erosion (element removal) when a specific strain value is reached. Thus, three performances are considered: completely disabled erosion (**`EROD < 1.0`**), enabled erosion for a completely damaged concrete material with an effective strain of 5% (**`EROD = 1.05`**), and the previous variant, but with replacement of each removed solid element by a discrete element sphere (DES particle) – a simplified version of discrete element method (DEM). This is possible thanks to the use of the **`*DEFINE_ADAPTIVE_SOLID_TO_DES`** card. The DES particle behavior parameters are set for dry send (see Table 3) [11].

Table 3: Parameters for discrete elements

`*CONTROL_DISCRETE_ELEMENT`							
`$#`	**`ndamp`**	**`tdamp`**	**`fric`**	**`fricr`**	**`normk`**	**`sheark`**	**`cap`**	**`mxnsc`**
	0.5	0.5	0.57	0.1	0.01	0.0029	0	0

The fixing of the RC plate on the stand is modeled by prohibiting any movement of the supporting steel plates on the back side of the model. The LED model strikes the center of the plate with an initial velocity of 214 m/s. Gravity is not considered because its influence is negligible.

3.3 Contacts and couplings

The model utilizes many contact interactions of different natures. First, all beam parts immersed in concrete are coupled using the constrained equations created by the **`*CONSTRAINED_BEAM_IN_SOLID`** card. As shown earlier [10], the coupling created in this way does not differ from the merging of solid and beam mesh nodes but significantly simplifies model development.
The steel support plates are joined to the anchor rods through common nodes. **`*CONTACT_TIED_NODES_TO_SURFACE`** defines the contact interaction between the plates and the concrete. Thus, the adhesion between the plates' metal and the concrete is assumed to be perfect.
The contact interaction between the concrete and all LED parts is defined by **`*CONTACT_AUTOMATIC_SINGLE_SURFACE, SOFT=2`**. This set of contact interactions should be sufficient to simulate the system's behavior without eroding the concrete elements. For the scenario with element erosion, it is possible to switch to the **`ERODIN`** version of the contact card, but it is not too important, because when removing concrete elements, the projectile will interact already with the rebar.

However, other contact interactions must be considered if erosion is included. For example, in the case of concrete erosion and exposed reinforcement, its bars should interact with each other via ***CONTACT_AUTOMATIC_GENERAL** and with deformed LED via ***CONTACT_AUTOMATIC_BEAMS_TO_SURFACE**.
In the case of substitutions of remote concrete elements, the contact interactions of the model with spherically discrete elements need to be considered. It is necessary to consider the interaction of the continuously generated DES in the continuously deteriorating FE concrete via ***CONTACT_ERODING_NODES_TO_SURFACE** and with the LED model via ***CONTACT_AUTOMATIC_NODES_TO_SURFACE**. For realistic DES to FE contact interaction in classical contacts, increasing the penalty coefficients on the FE side by a factor of 60 is necessary. It is also recommended to set **FS = 0.6**, **FD = 0.4** [11].
As shown [12], when modeling plane concrete, replacing removed solid elements with SPH particles allows a perfect agreement with the experiment. At the same time, the calculation shows low sensitivity to the material removal parameters and FE element size. However, this approach cannot be applied in calculations where the interaction of the crushed concrete with the reinforcement mesh must be considered. An essential feature of switching eroded FE solids to DES instead of SPH is the ability to include DES-to-beams interaction via ***DEFINE_DE_TO_BEAM_COUPLING, FRICS=FRICD=0.45, DAMP = 0.5, BSORT = 100**, which allows realistic retention of concrete fragments inside the reinforcement cage.

4 Simulation results

Measurement of forces and stresses in concrete structures can cause difficulties with mathematical modeling and processing experimental data. The deformations and the local failure status are of greater practical importance in the study of reinforced concrete slabs after impacts. Classification of local effects observed during impact impacts on reinforced concrete structures according to the Nuclear Energy Institute (NEI) [13] can be seen in Fig. 11:

- penetration – the displacement of the projectile into the target;
- spalling – the ejection of target material from the front face of the target;
- scabbing – the ejection of material from the back face of the target;
- perforation – the projectile thoroughly penetrates and passes through the target.

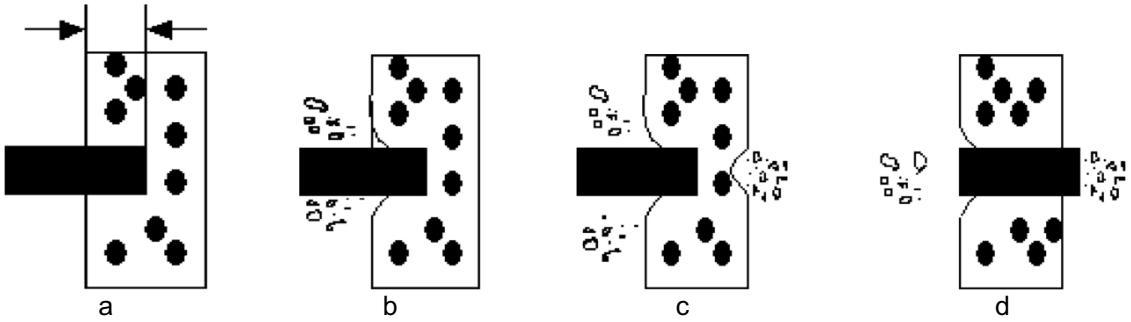

Fig.11: Classification of the local effects observed during impact on RC structures according to NEI [13]: a – penetration; b – spalling; c – scabbing; d – perforation.

Thus, the calculation results will be compared with the experimental data on the displacements of critical points of the slab's rear surface (see Fig. 12) at certain moments. After that, the model's state will be shown to determine the local failure pattern.

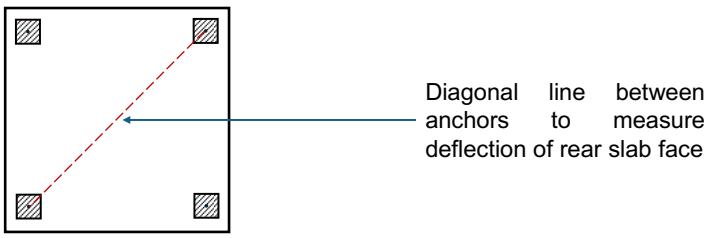

Fig.12: Diagonal line between anchors to measure the deflection of rear slab face

4.1 Slab rear face deflection for the model without material erosion

The use of erosive material is very complex and always a one-size-fits-all decision. Examples can be found in the literature [14], where the element removal criterion was an additional parameter to fit the model performance to a known material. Thus, the model could perfectly describe the available data but lost most of its predictive ability. Therefore, the first vergence of the computation is performed without using the element removal technique.

The calculation with disabled element erosion shows a behavior observed before [10]. The CSCM material exploits the principles of damage mechanics and simulates the failure of concrete by softening. However, the softened material loses its strength, not mass. The experiment considers a relatively long-time-interval: an elastic wave passes through the plate in about 0.43 ms, and we consider results for 25 ms. During such a long-time interval, the softened material inevitably has time to deform under the action of inertial forces.

Observations show that the finer the mesh we use, the worse the accuracy of the results. Several factors explain this. Suppose the element size is relatively large (comparable to the reinforcement spacing). In that case, no fully softened concrete elements are formed—the FE model is too coarse to describe such a local effect.

Further, as the element size decreases, the cage of rebars can compensate for the behavior of the softened material.

However, as soon as the size of concrete elements becomes comparable to the thickness of the concrete cover layer (60 mm), a complete layer of unreinforced elements is formed on the slab's surface. Once they have been softened, nothing can stop them from deforming unphysically under the action of inertial forces.

This behavior is observed in Figure 13. The models with 200 mm and 150 mm element sizes cannot describe the nonlinear behavior of the structure, especially in the central region, directly under the impact point. It coincidentally coincides with the experimental results. As the element size decreases, there is a rapid increase in the displacements at the rear surface, which is especially visible at time 20 - 25 ms (see Fig. 13 d - e). Thus, the model without element erosion strongly depends on the size of the FE mesh.

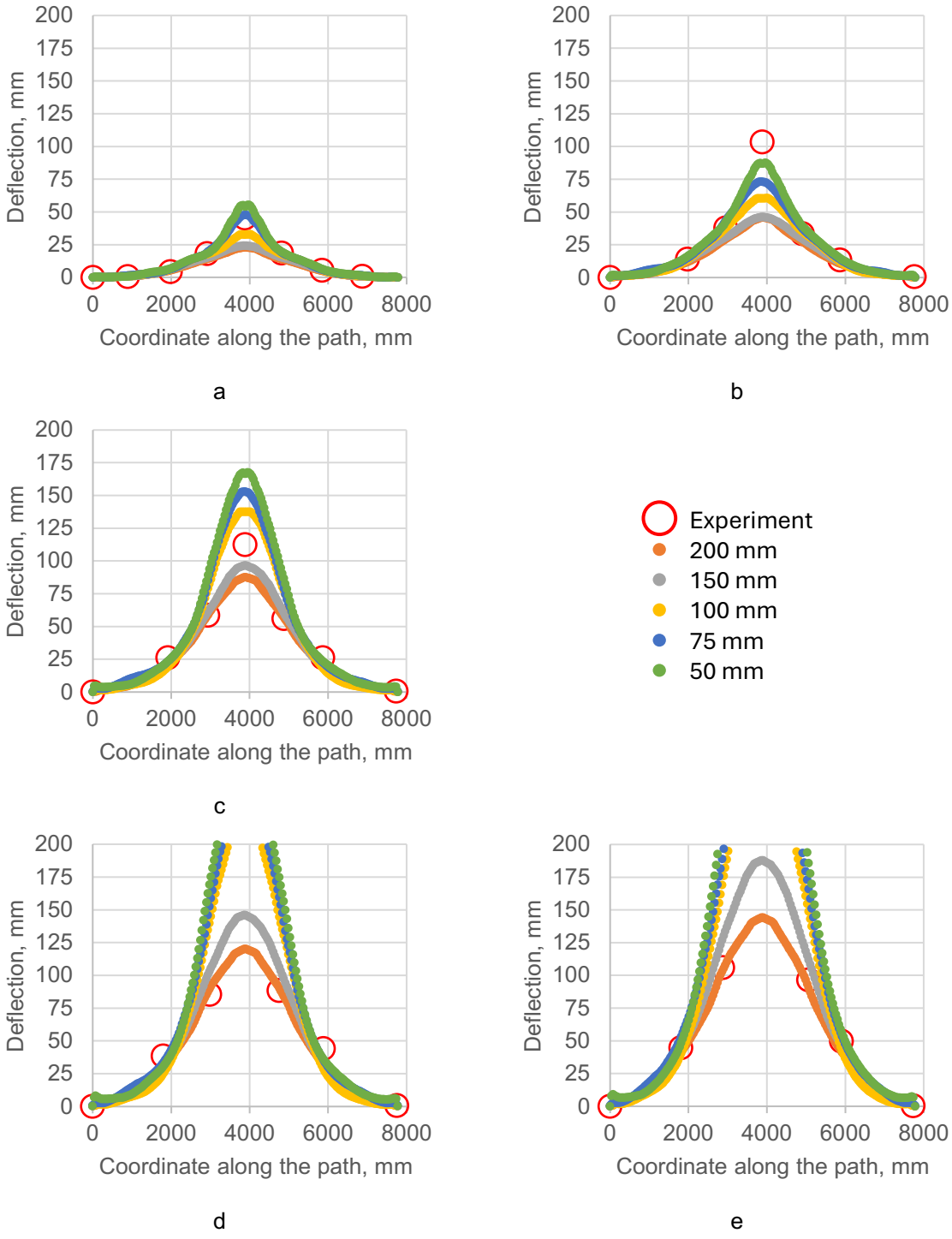

Fig.13: Displacements on the diagonal line of the back surface of the slab at key moments: a – 5 ms; b – 10 ms; c – 15 ms; d – 20 ms; e – 25 ms.

4.2 Slab rear face deflection for the model with material erosion

Removing elements according to the strain-based criterion is the most straightforward mechanism to compensate for the softened material's unphysical behavior. Determining the criterion by which the removal of elements occurs is a complex task. For example, the NEI [13] defines a maximum shear strain of 0.5% as a criterion for concrete separation. However, we cannot directly use this value since the damage accumulation and softening mechanism already account for part of the concrete fragmentation process.

It is essential to understand that the erosion criterion for FE calculations with material models that use damage is not a means of describing material failure but rather a means of dealing with undesirable numerical effects in a softened material. Thus, to study the influence of the erosion parameter, we chose the value of 5% strain (`erod = 1.05`) since it is often used by the model's authors in its verification manual [15].

Figure 14 shows the simulation results. The model now shows significantly smaller rear surface displacements, especially when using small element sizes. Removing elements corrects the previously observed undesirable effects.

However, although the solution becomes more robust to changes in mesh size, it still does not show a monotonic dependence on mesh size. The displacements increase as the mesh size decreases from 200 mm to 100 mm, but then, starting size 75 mm, they decrease. This can be seen particularly well in Figure 15e. It can be assumed that along with the model, it also loses momentum and energy while removing elements. When the mesh is used, more elements are removed, and there is a more significant underestimation of the load on the model.

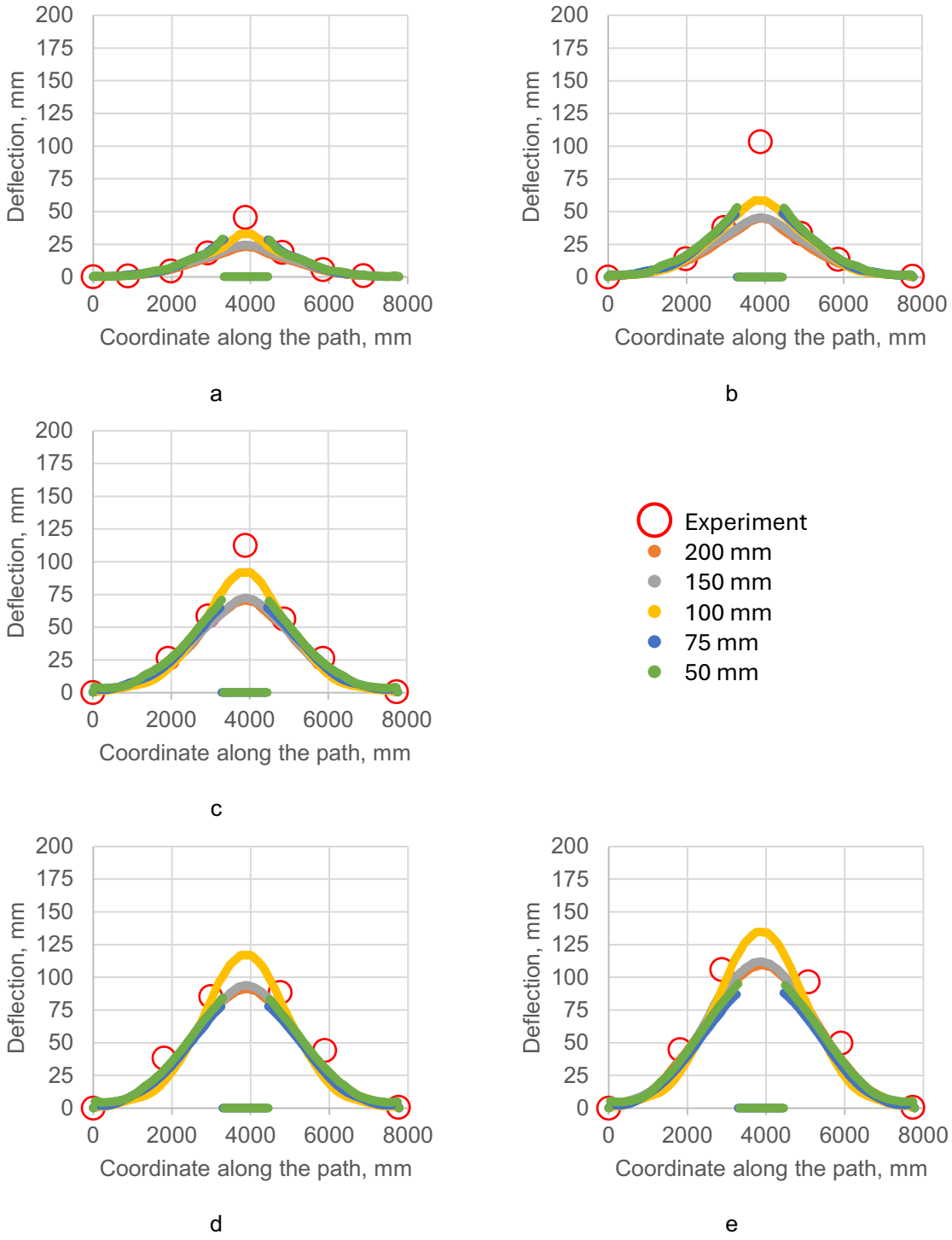

Fig.14: Displacements on the diagonal line of the back surface of the slab at key moments: a – 5 ms; b – 10 ms; c – 15 ms; d – 20 ms; e – 25 ms.

4.3 Slab rear face deflection for the model with material erosion and adaptive switching to DES

Let us study the model's performance when adaptive switching of deleted concrete finite elements to DES is implemented. The concrete material model is still configured so that the element is removed when the strain threshold of 5% is reached for maximally softened concrete. However, the solver now creates a discrete (rigid sphere) element instead of the deleted element. The created discrete element inherits the dimensions, mass, and momentum from the removed finite element.
The approach with adaptive FE switching in the DES allows us to significantly improve the preservation of mass and momentum balance while avoiding undesirable effects of distortion of the FE mesh by softened material. This approach is the simplest way to initially assess the dynamic behavior of debris in a fragmented structure.
The model using the described technique shows more consistent results (see Fig. 15). As the element size decreases, the plate's back surface displacements gradually approach the experimental measurements. However, the rear surface displacements remain unchanged from an element size of 100 mm up to the most detailed grid of 50 mm. This allows us to verify the stability of the solution and obtain practical mesh convergence. Now, the element size from 75 mm to 100 mm is sufficient to accurately describe the condition of the concrete slab in this experiment.

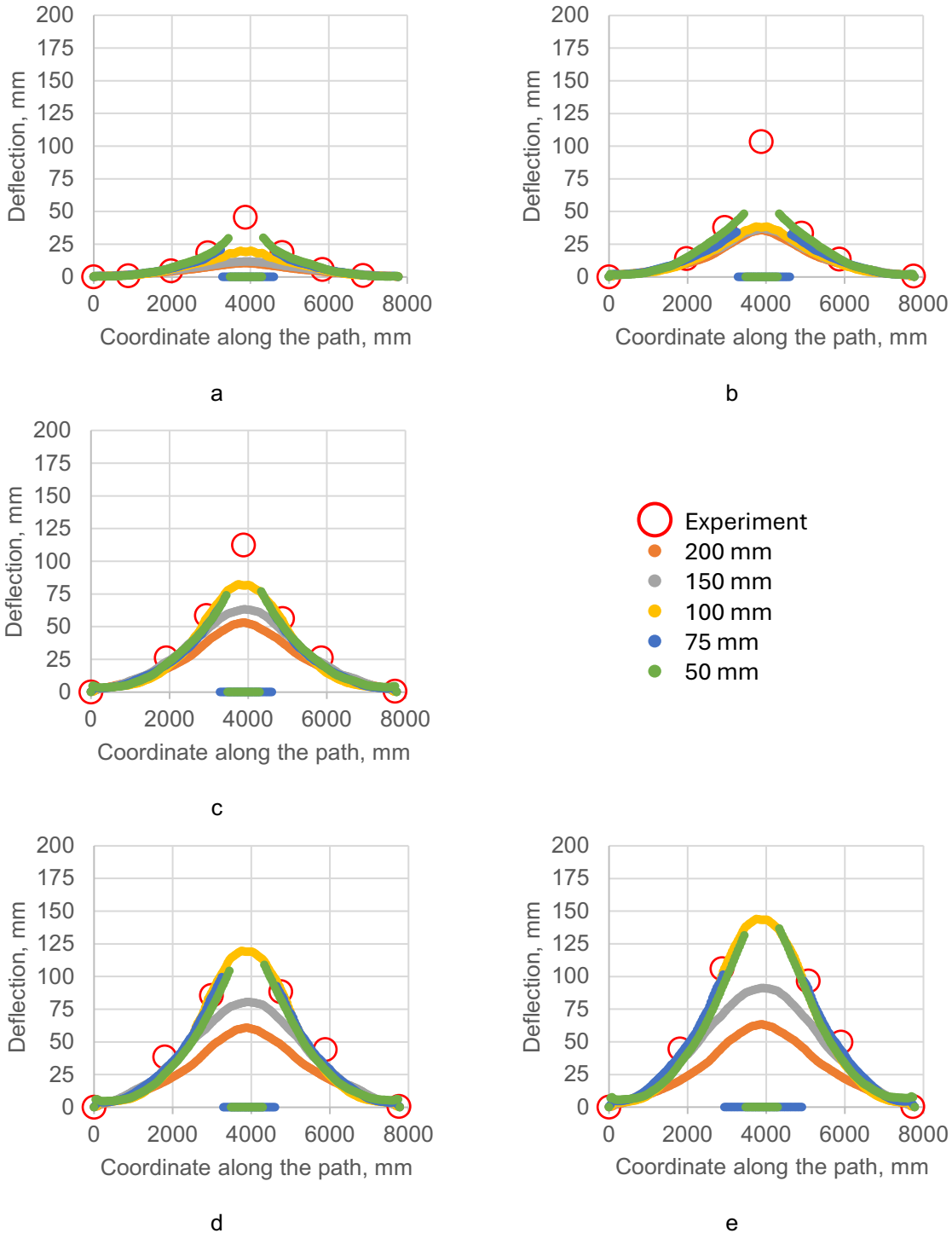

Fig.15: Displacements on the diagonal line of the back surface of the slab at key moments: a – 5 ms; b – 10 ms; c – 15 ms; d – 20 ms; e – 25 ms.

4.4 Local slab failure comparison for different assumptions

Let's compare the three modeling approaches for an element size of 75 mm, which is larger than the thickness of the concrete pavement, which means all three approaches should work. We will consider the damage field for the deformed state of the model at the moment of impact termination (t = 100 ms). First, let's pay attention to the frontal face. The volume of elements with maximal concrete damage for the model with disabled erosion is the largest (see. Fig. 16a). The crater formed under the impact site is also visible. The reinforcing bars are exposed under the impact point for the model with erosion enabled, and all the concrete around them has been removed (see. Fig. 16b). This model condition shows improper load distribution. The model using DES switching shows an intermediate state: a crater is visible, and some of the reinforcement is exposed due to the spalling of the concrete cover (see Fig. 16c). But behind the reinforcement, there are still uncorroded concrete elements.

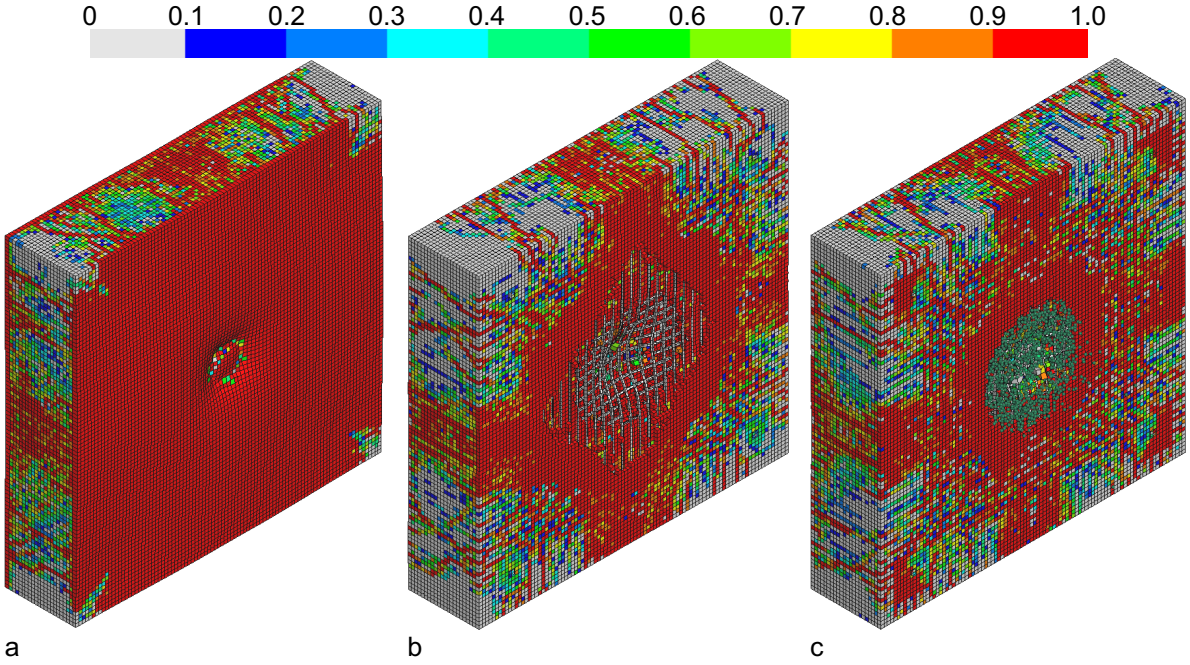

Fig.16: RC slab front face after impact (t = 100 ms, element size 75 mm), damage: a – without material erosion; b – with material erosion; c – adaptive switching to DES

It is known from experimental data that after the impact, a crater with a depth of about 210 mm was formed on the surface of the plate. This value can be compared with the results of calculations (see Table 4, Fig. 17). Without considering erosion, the model significantly underestimates the crater depth, as it cannot effectively simulate concrete spalling using only the softening mechanism. Moreover, as the element size decreases, the model's already mentioned "swelling" is observed: maximally softened concrete elements on the damage begin to deform along the impact direction under the action of inertial forces.

On the contrary, the model that included element removal overestimates the crater depth. We noted above that the volume of removed concrete within the model is too large. The model switching the removed elements in DES shows excellent agreement with the experiment with an error of about 5%.

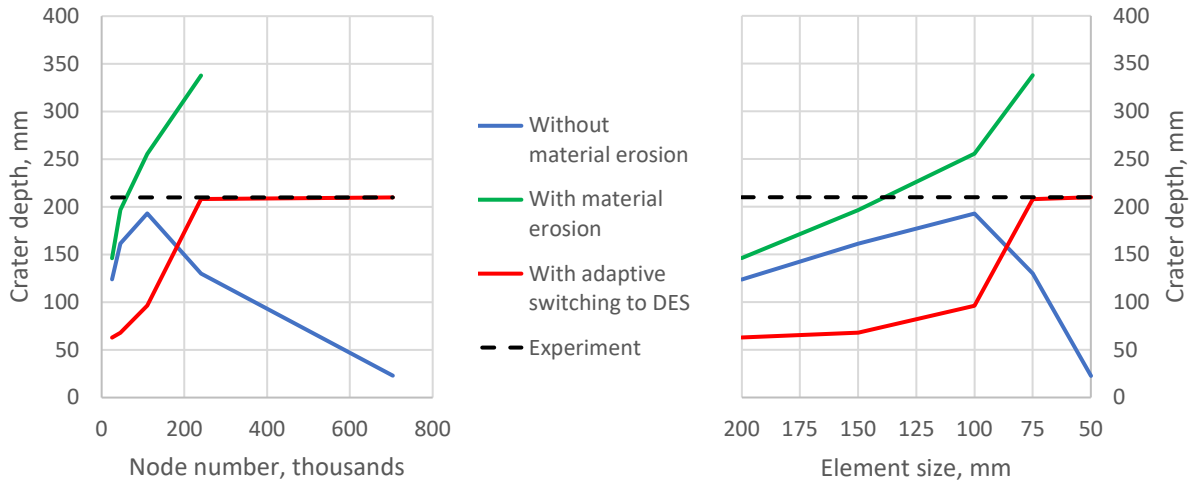

Fig.17: The front slab face crater estimation: a – dependence of crater depth on the FE model nodes number; b – dependence of crater depth on the FE model element size

Table 4: The front slab face crater estimation for element size 75 mm

	Crater depth, mm	Crater depth estimation error
Without material erosion	146.3	-44%
With material erosion	337.8	38%
With adaptive switching to DES	221.5	5%
Experiment	210.0	-

We can also visually compare the condition of the rear surface of the slab after impact with the experiment's results. Only the model with adaptive switching in DES can show the correct deposition of the concrete coating on the rear face (see Fig. 18c). At the same time, the model without erosion shows a significant deflection and damage of the rear surface (see Fig. 18a). The slab “swells” after impact. For the models with erosion included, there is an overestimation of the concrete settlement volume, and the pitting area does not match the experimental results in terms of shape or area (see Fig. 18b).

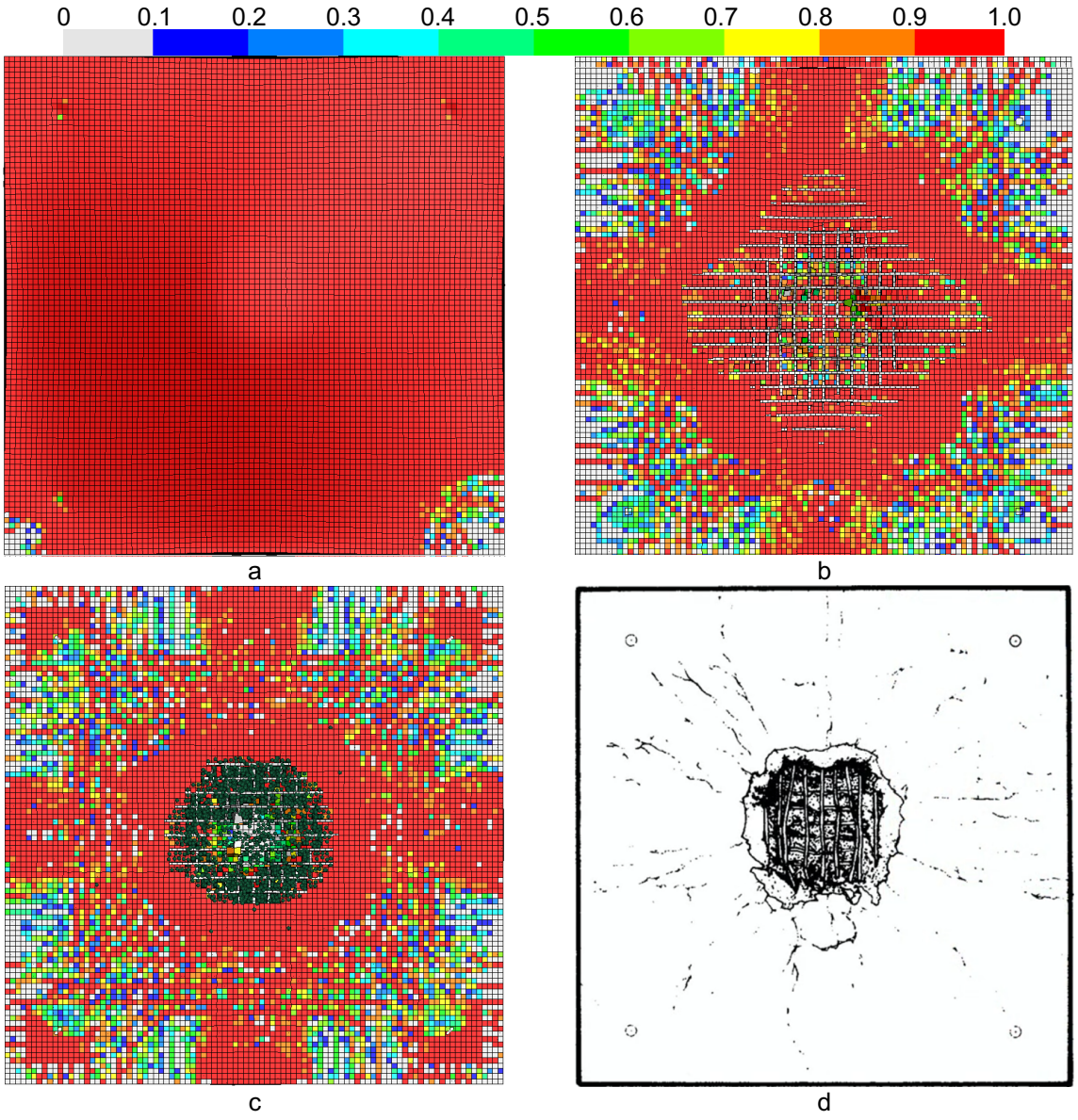

Fig.18: RC slab rear face after impact (t = 100 ms, element size 75 mm), damage: a – without material erosion; b – with material erosion; c – adaptive switching to DES, d – experimental results

The results show that the model with adaptive switching in DES shows scabbing behavior, as in the experiment. The model with erosion is on the boundary between scabbing and perforation. The model must have erosion to give correct results about the local state of the concrete slab.

5 Summary

An approach to modeling the fragmentation of reinforced concrete under high-intensity loads is considered. This approach involves automatically switching damaged and significantly deformed concrete elements to the calculation by the DES method. This allows not only to improve compliance with the laws of conservation of mass and momentum but also to achieve practical mesh convergence. Thus, we can determine the required element size to describe the nonlinear behavior of the structure being destroyed without directly adjusting the experiment. Such a technique can be applied to modeling a wide range of impact loads. It is recommended for modeling reinforced concrete structures since it allows considering the interaction of debris not only with undestroyed material but also with the cage formed by the rebars.

6 Literature

[1] Novozhilov, Y., et al., "Aircraft NPP Impact Simulation Methodology," 16-th International LS-DYNA Conference, 2020, https://www.dynalook.com/conferences/16th-international-ls-dyna-conference/simulation-t9-2/t9-2-e-simulation-096

[2] Sugano, T. et al., "Local damage to reinforced concrete structures caused by impact of aircraft engine projectiles Part 1. Test program, method and results," Nuclear Engineering and Design, https://doi.org/10.1016/0029-5493(93)90120-X

[3] Sugano, T., et al., "Local damage to reinforced concrete structures caused by impact of aircraft engine projectiles Part 2. Evaluation of test results," *Nuclear Engineering and Design*, https://doi.org/10.1016/0029-5493(93)90121-O

[4] Muto, K., et al., "Experimental Studies on Local Damage of reinforced concrete Structures by the Impact of Deformable Projectiles Part 1: Outline of Test Program and Small-Scale Tests," In Transactions of the 10th SMiRT (pp. 257–264). http://www.iasmirt.org/transactions/10/DC_250396.pdf

[5] Esashi, Y., et al., "Experimental Studies on Local Damage of reinforced concrete Structures by the Impact of Deformable Projectiles, Part 2: Intermediate Scale Tests, "*Transactions of the 10th SMiRT*, 265–270. https://repository.lib.ncsu.edu/handle/1840.20/29541

[6] Muto, K., et al., "Experimental Studies on Local Damage of reinforced concrete Structures by the Impact of Deformable Projectiles Part 3: Full Scale Tests, " In *Transactions of the 10th SMiRT* (pp. 271–278). http://www.iasmirt.org/transactions/10/DC_250398.pdf

[7] Muto, K., et al., "Experimental Studies on Local Damage of reinforced concrete Structures by the Impact of Deformable Projectiles Part 4: Overall Evaluation of Local Damage, "In *Transactions of the 10th SMiRT* (pp. 279–284). http://www.iasmirt.org/transactions/10/DC_250399.pdf

[8] Novozhilov, Y., et al., "Precise Calibration of the Continuous Surface Cap Model for Concrete," Simulation. Buildings, 12(5), 2022, https://doi.org/10.3390/buildings12050636

[9] IAEA, Safety Reports Series No. 87: Safety Aspects of Nuclear Polter Plants in Human Induced External Events: General Considerations. 2017, https://www-pub.iaea.org/MTCD/publications/PDF/PUB1769_web.pdf

[10] Novozhilov, Y., et al., "Aircraft NPP Impact Simulation Methodology, " 16-Th International LS-DYNA Conference, 2020. https://www.dynalook.com/conferences/16th-international-ls-dyna-conference/simulation-t9-2/t9-2-e-simulation-096.pdf/view

[11] Karajan, N., et al., "Particles as Discrete Elements in LS-DYNA: Interaction with themselves as well as Deformable or Rigid Structures," 11-th LS-DYNA Forum, Ulm, 2012, https://www.dynalook.com/conferences/9th-european-ls-dyna-conference/interactionpossibilities-of-bonded-and-loose-particles-in-ls-dyna-r

[12] Dmitriev, A., et al., "Simulation of Concrete Plate Perforation by Coupled Finite Element and Smooth Particle Hydrodynamics Methods," Construction of Unique Buildings and Structures, 92(9207) 2020, https://doi.org/10.18720/CUBS.92.7

[13] Nuclear Energy Institute, "Methodology for Performing Aircraft Impact Assessments for New Plant Designs (NEI 07-13 Revision 8P)" (Issue April 2011). https://www.nrc.gov/docs/ML1114/ML111440006.pdf

[14] Luccioni, B., et al., "Erosion Criteria for Frictional Materials Under Blast Load", Mecánica Computacional, XXX, 1809–1831.

[15] Murray, Y. D., et al., "Evaluation of LS-DYNA Concrete Material Model 159. In Federal Highway Administration", (2007), https://www.fhwa.dot.gov/publications/research/infrastructure/structures/05063/05063.pdf